Heat Transfer From Air-Cooled Contrarotating Disks

J.-X. Chen

X. Gan[1]

J. M. Owen

School of Mechanical Engineering,
University of Bath,
Bath, United Kingdom

A superposed radial outflow of air is used to cool two disks that are rotating at equal and opposite speeds at rotational Reynolds numbers up to 1.2×10^6. One disk, which is heated up to 100°C, is instrumented with thermocouples and fluxmeters; the other disk, which is unheated, is made from transparent polycarbonate to allow the measurement of velocity using an LDA system. Measured Nusselt numbers and velocities are compared with computations made using an axisymmetric elliptic solver with a low-Reynolds-number $k-\epsilon$ turbulence model. Over the range of flow rates and rotational speeds tested, agreement between the computations and measurements is mainly good. As suggested by the Reynolds analogy, the Nusselt numbers for contrarotating disks increase strongly with rotational speed and weakly with flow rate; they are lower than the values obtained under equivalent conditions in a rotor–stator system.

1 Introduction

In most gas turbines, a turbine disk rotates close to either a stationary casing or another corotating turbine disk. In some engines, and in some designs of future engines, two adjacent disks may rotate in opposite directions. Such contrarotating turbines could be used to drive the contrarotating fans of future generations of ultra-high-bypass-ratio engines, and an additional advantage is that contrarotating turbine stages remove the need for an intermediate row of stator vanes, thereby reducing the size and weight of the engine.

Recent research in contrarotating disks has produced a number of papers, most of which are concerned with the fluid dynamics of the problem. Graber et al. (1987) reported extensive experimental measurements obtained from a pressurized rotating-disk rig in which the two disks could be rotated, in either direction, to produce rotational Reynolds numbers up to $\mathrm{Re}_\phi = 1.6 \times 10^7$, typical of those found in gas turbines. For their contrarotating-disk tests, a *stationary* shroud (or cylindrical casing) was used to seal the periphery of the system. A superposed radial inflow or outflow of air could be supplied, and the measurements of frictional moment coefficients, C_m, on one of the rotating disks, showed that neither the magnitude nor the direction of the flow rate had a significant effect on C_m. However, the value of C_m for a contrarotating disk with no superposed flow is approximately twice that of the equivalent rotor-stator case, where one disk is rotating and the other is stationary.

Morse (1991) and Kilic et al. (1996) carried out computations for the contrarotating-disk case using elliptic solvers and (different) low-Reynolds-number $k-\epsilon$ turbulence models. Their computed moment coefficients were in close agreement with each other and with the correlation of Dorfman (1963) for the free-disk case (that is, a single disk rotating in a quiescent environment), where

$$C_m = 0.491\ (\log_{10} \mathrm{Re}_\phi)^{-2.58} \qquad (1.1)$$

Like the experiments of Graber et al. the computations showed that, with no superposed flow, the moment coefficients for contrarotating disks are approximately twice those of the rotor–stator case. However, whereas a superposed radial outflow has little effect on C_m for contrarotating disks, it has a large effect for the rotor–stator system. In the latter case, C_m approaches the free-disk value (and consequently, the contrarotating-disk value) as the flow rate approaches the free-disk entrainment rate (that is, the flow rate entrained by the free disk).

A combined computational and experimental study of the flow and heat transfer associated with air-cooled contrarotating disks has recently been completed at the University of Bath. Velocity and heat transfer measurements were obtained for rotational Reynolds numbers up to $\mathrm{Re}_\phi \simeq 1.2 \times 10^6$ over the range $-1 \le \Gamma \le 0$, where Γ is the ratio of the speed of the slower disk to that of the faster one: $\Gamma = 0$ corresponding to the rotor–stator case and $\Gamma = -1$ to disks rotating at equal and opposite speeds. Computations of the flow were made using an elliptic solver with a low-Reynolds-number $k-\epsilon$ turbulence model, and further details of the computed and measured flows are given by Gan et al. (1995) and by Kilic et al. (1994a, b, 1996). The principal features of the flow are outlined below, and the flow structures for $\Gamma = 0$ and $\Gamma = -1$ are shown schematically in Fig. 1.

When there is no superposed flow between the disks, then, depending on the value of Γ, Batchelor-type flow (Batchelor, 1951) or Stewartson-type flow (Stewartson, 1953) can occur. For $\Gamma = 0$, Batchelor-type flow comprises radial outflow in a boundary layer on the rotating disk (the rotor), and radial inflow in a boundary layer on the stationary disk (the stator); between the boundary layers is a core of rotating fluid in which the radial component of velocity is zero and there is an axial flow from the stator to the rotor. For $\Gamma = -1$, Stewartson-type flow comprises a radial outflow in boundary layers on both disks, between which is a recirculating core of fluid that is entrained into the outflowing boundary layers; the tangential component of velocity in this core is very small.

For contrarotating disks there is a double transition: from laminar to turbulent flow and from Batchelor-type to Stewartson-type flow, depending on Γ and Re_ϕ. For $\Gamma = 0$, transition from laminar to turbulent Batchelor-type flow occurs at $x^2\mathrm{Re}_\phi \simeq 2 \times 10^5$. For $\Gamma = -1$, laminar flow can occur in the boundary layers but, even at local Reynolds numbers as low as $x^2\mathrm{Re}_\phi = 2 \times 10^4$, the flow in the core always appears to be turbulent. (For $\Gamma = -1$, laminar Batchelor-type flow can be computed but it appears not to exist in practice.) For $-1 < \Gamma < 0$, a two-cell structure can occur: Batchelor-type flow with a rotating core occurs in the (radially) outer cell, and Stewartson-type flow with a nonrotating recirculating core occurs in the inner cell.

[1] Present address: European Gas Turbines Ltd, Whetstone, Leicester LE8 6LH, United Kingdom.

Contributed by the International Gas Turbine Institute and presented at the 40th International Gas Turbine and Aeroengine Congress and Exhibition, Houston, Texas, June 5–8, 1995. Manuscript received by the International Gas Turbine Institute February 22, 1995. Paper No. 95-GT-184. Associate Technical Editor: C. J. Russo.

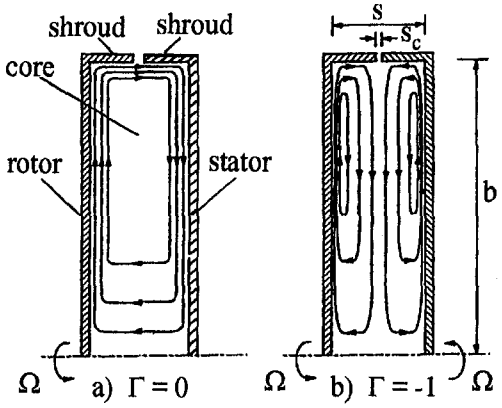

Fig. 1 Schematic diagram of flow structure (no superposed flow)

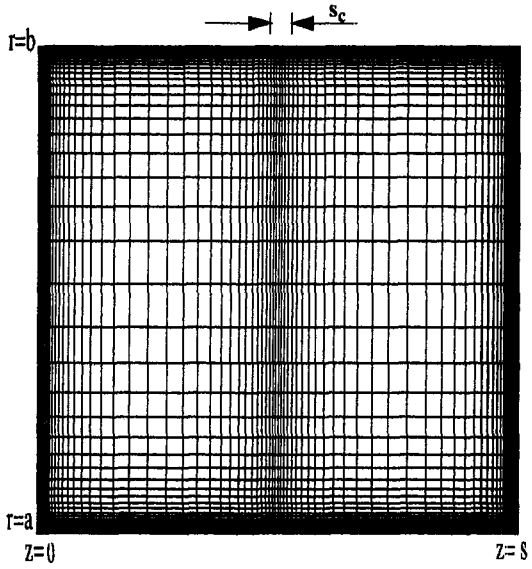

Fig. 2 Typical computational grid (92 radial × 78 axial nodes) (not to scale)

For $\Gamma = -1$, a superposed radial outflow of fluid divides the flow structure into two regions: a source region near the inlet, where fluid is entrained into a free-disk-type boundary layer on each disk, and an outer recirculating region where Stewartson-type flow occurs. The nondimensional flow rate, C_W, entrained by the turbulent free disk can be approximated by

$$C_W = 0.22\ \mathrm{Re}_\phi^{0.8} \tag{1.2}$$

It is convenient to define the turbulent flow parameter, λ_T, as

$$\lambda_T = C_W\ \mathrm{Re}_\phi^{-0.8} \tag{1.3}$$

where $\lambda_T = 0.22$ corresponds to the free-disk entrainment rate; in most turbine-disk cooling applications, $\lambda_T < 0.22$. Gan et al. (1995), using an argument based on free-disk entrainment in the source region, suggested that the nondimensional radius of the source region, x_e, could be approximated by

$$x_e = 1.37\ \lambda_T^{0.385} \tag{1.4}$$

These papers were concerned with the fluid dynamics of the problem, whereas this one concentrates principally on the heat transfer from contrarotating disks for $\Gamma = -1$. The computational method and experimental apparatus are outlined in Sections 2 and 3, and the comparisons between computations and measurements are discussed in Section 4.

2 Computational Method

An "in-house elliptic code" was used to solve the incompressible, axisymmetric, conservation equations for mass, momentum, energy, and turbulence quantities together with a low-Reynolds-number $k-\epsilon$ turbulence model (Morse, 1988, 1991). Turbulent heat fluxes were computed from the temperature gradients using a turbulent Prandtl number. The code has been used successfully to compute the flow and heat transfer for the free-disk case and for rotor-stator systems; details are given by Chen et al. (1993a, b, 1996).

A typical grid distribution for the contrarotating disks is shown in Fig. 2. For most tests, a nonuniform grid with 92 radial and 78 axial nodes was used, and a geometric expansion/contraction factor was employed to achieve a fine grid near the disks: for all computations reported here, the grid point closest to the disk was set to ensure that $y^+ < 1.0$. Grid-independence tests were conducted by making computations with a fine (92 × 78) and a coarse (68 × 68) grid: There was no graphic difference between the two sets of velocity profiles and the Nusselt numbers differed by less than 2 percent.

In the experiments, the disks were spaced a distance s apart and flow entered the system at $r = a$ through a gauze tube attached to each disk (see Section 3) and left through a small axial clearance, s_c, between the contrarotating shrouds at $r =$

Nomenclature

a = inner radius of disk
b = outer radius of disk
C_m = moment coefficient = $M/0.5\ \rho\Omega^2 b^5$
C_p = specific heat at constant pressure
C_w = nondimensional mass flow rate = $\dot{m}/\mu b$
G = gap ratio = s/b
G_c = shroud-clearance ratio = s_c/b
k = thermal conductivity; turbulent kinetic energy
$\dot{m}$ = mass flow rate
M = moment on rotating disc
Nu = Nusselt number = $q_o r/k(T_o - T_{\mathrm{ref}})$
Pr = Prandtl number of air
q_o = convective heat flux from disk to air
r = radial coordinate
R = recovery factor
Re_ϕ = rotational Reynolds number = $\rho\Omega b^2/\mu$
s = axial gap between disks
s_c = shroud clearance
T = temperature
U_τ = friction velocity = $\sqrt{(\tau_w/\rho)}$
V_r, V_ϕ, V_z = velocity components in r, ϕ, z directions
x = nondimensional radius = r/b
x_e = nondimensional radius of source region
y = distance normal to wall
y^+ = wall-distance Reynolds number = $\rho U_\tau y/\mu$
z = axial coordinate from heated disk
ϵ = turbulent energy dissipation rate
Γ = ratio of speed of slower disk to that of faster one
λ_T = turbulent flow parameter = $C_w \mathrm{Re}_\phi^{-0.8}$
μ = dynamic viscosity
ϕ = tangential coordinate
ρ = density
τ_w = total wall shear stress
Ω = angular speed of disc

Subscripts

ad = adiabatic value
I = inlet value
o = surface of rotating disk
ref = reference value
1, 2 = unheated, heated disk

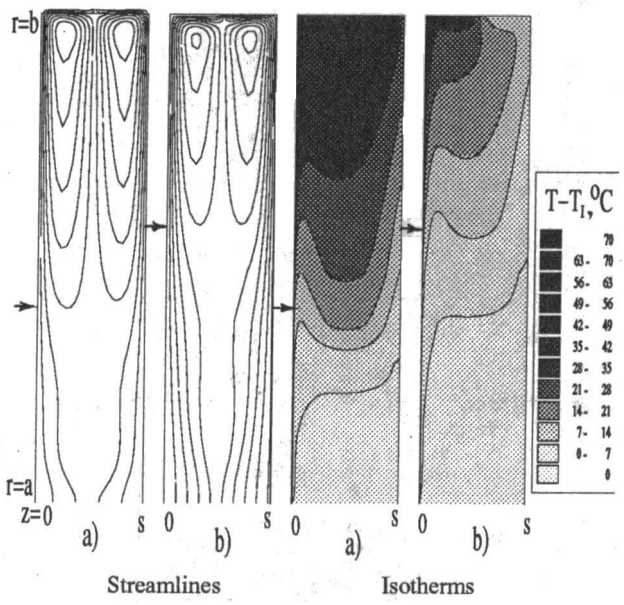

Fig. 3 Computed streamlines and isotherms for $\Gamma = -1$: (*a*) $C_W = 4026$, $Re_\phi = 1.14 \times 10^6$ ($\lambda_T = 0.0575$); (*b*) $C_W = 9351$, $Re_\phi = 1.19 \times 10^6$ ($\lambda_T = 0.129$); ↑ x_e (Eq. (1.4))

b. The computational geometry matched the experimental one: $a/b = 0.13$, $G = s/b = 0.12$, $G_c = s_c/b = 0.01$. No-slip conditions were used for the velocities on all solid surfaces, and at the inlet, $r = a$, the flow was assumed to enter uniformly in the radial direction and the inlet temperature, T_I, was specified; for $0 \leq z/s < \frac{1}{2}$, $V_\phi = \Omega a$, and for $\frac{1}{2} < z/s \leq 1$, $V_\phi = -\Omega a$. At the outlet, $r = b$, the flow was assumed to leave uniformly in the radial direction, and the radial derivatives of the tangential component of velocity and the temperature were assumed to be zero. In the experiment, only one disk was heated and thermocouples were used to measure its temperature; in the computations, the temperature of the heated disk was obtained using interpolation of the measured temperatures, and the unheated disk and shrouds were assumed to be adiabatic.

Computed streamlines and isotherms for $\Gamma = -1$ and $Re_\phi \simeq 1.1 \times 10^6$ are shown in Fig. 3 for the geometry and thermal conditions corresponding to the experimental apparatus; the left-hand disk is heated and the right-hand one is adiabatic. The streamlines show that the flow entering at $r = a$ forms a source region outside of which recirculation occurs. The arrows indicate the radial extent of the source region given by the free-disk-entrainment model, Eq. (1.4), which overestimates the computed size. The isotherms show that inside the source region the air temperature is equal to that at inlet, T_I, and outside recirculation causes the air temperature to increase with radius. At the larger radii, the temperature of the adiabatic disk is greater than T_I.

3 Experimental Apparatus

The apparatus, which is shown in Fig. 4, was essentially the same as that described by Chen et al. (1996) and so only the salient features are described here.

Two disks of 762 mm diameter were rotated independently at speeds up to 1500 rpm; the speed was measured with an uncertainty of 1 rpm. Disk 1, which was unheated, was made from transparent polycarbonate; disk 2, which could be radiantly heated, was made from steel. A carbon-fiber shroud was attached to the periphery of each disk, and the axial clearance between the contrarotating shrouds was less than 4 mm ($G_c \simeq 0.01$); the axial spacing between the two disks was approximately 46 mm ($G \simeq 0.12$).

A radial outflow of air could be supplied through rotating gauze tubes of 100 mm diameter ($a/b \simeq 0.13$) attached to the center of the disks (see Fig 4). The air was supplied to the rig from a centrifugal compressor, via a stationary and a rotating tube attached to the center of the upstream disk. The flow rate was measured, with an uncertainty of around 3 percent, using an orifice plate in the stationary tube; leakage was minimized by the use of seals between the stationary and rotating tubes. It should be pointed out that the gauze tubes were intended to produce a uniform radial flow at inlet to the system; velocity measurements showed that this was not achieved.

The back face of the steel disk (disk 2) could be heated electrically by stationary radiant heaters to produce a maximum temperature of approximately 100°C (around 70°C above that of the cooling air at inlet). Ten thermocouples and ten RDF thermopile fluxmeters (three of which subsequently broke) were embedded in a glass-fiber "mat," 0.8 mm thick, bonded to the front face of the disk. The signals were taken out through an IDM slip-ring assembly, and the voltages were measured in a Schlumberger computer-controlled data-logger. By taking the average of 100 sets of data, the random uncertainties were 0.03°C for the thermocouple readings. The overall uncertainties were estimated to be around 0.5°C for the thermocouples and 5 percent for the flux meters. (Chen et al., 1996, show good agreement between measured and computed Nusselt numbers for the free-disk case, which gives confidence in the accuracy of the fluxmeter measurements.)

The reference temperature, T_{ref}, used in the definition of the Nusselt number (see Nomenclature) was based on the *adiabatic-disk-temperature*, $T_{o,ad}$, employed by Chen et al. (1996) for their rotor–stator experiments:

$$T_{ref} = T_{o,ad} = T_I + \tfrac{1}{2} R\Omega^2 r^2 / C_p \qquad (3.1)$$

R being the recovery factor ($R \simeq Pr^{1/3}$). Ideally, the adiabatic-disk temperature should be based on the *local* air temperature and the *local* velocity difference ($\Omega r - V_\phi$), but it was only possible to measure the inlet air temperature, T_I, in the experiments. In practice, $\Omega^2 r^2 / 2C_p \leq 1$°C, but, as shown below, the computed difference between the local air temperature and T_I can be significant.

Radiation from the heated disk was also significant and it was necessary to estimate a correction for the radiative flux. The glass-fiber mat had an emissivity of approximately 0.95, and the fluxmeters measured the total heat flux (convection and

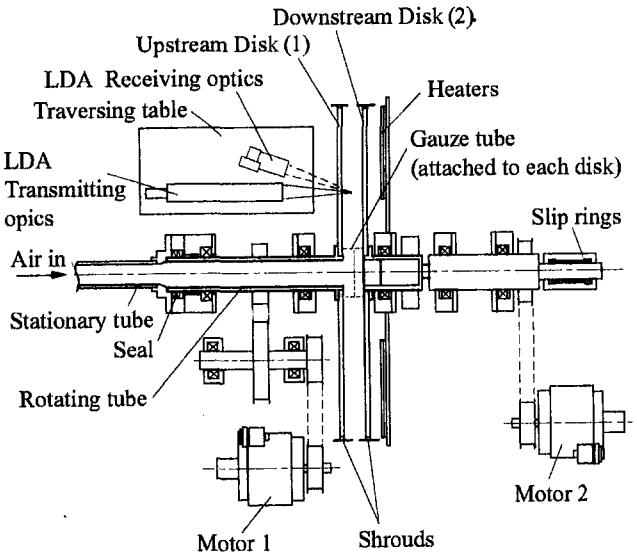

Fig. 4 Schematic layout of the rotating-disk rig and LDA system

radiation). Chen et al. (1996) assumed that the polycarbonate disk was opaque to infrared radiation and that its temperature (which was not measured) was equal to that of the cooling air at inlet. Using these assumptions, they estimated the radiative heat flux from the steel disk and produced corrections for the measured flux. In practice, the corrections, which can be as large as 10 percent of the measured flux, are likely to be overestimates of the radiation as the temperature of the polycarbonate disk can be higher than that of the cooling air (as discussed in Section 2).

The radial and tangential components of velocity were measured using a TSI laser-Doppler anemometer (LDA) operating in an off-axis back-scatter mode with the optical axis normal to the transparent polycarbonate disk. The Doppler frequency was measured with an IFA 750 burst correlator, and the estimated uncertainty in the measured tangential component of velocity was less than 0.5 percent of the disk speed. Positional uncertainty and scatter from the disk surfaces made it difficult to obtain accurate measurements close to either disk, particularly the steel one.

4 Comparison Between Computations and Measurements

4.1 Velocity Measurements. The radial and tangential components of velocity were measured at $x = 0.6, 0.7, 0.8$, and 0.85 for $2500 \leq C_W \leq 9700$ and $1.3 \times 10^5 \leq \mathrm{Re}_\phi \leq 1.3 \times 10^6$ ($0.05 \leq \lambda_T \leq 0.3$). Many comparisons between computations and measurement for the case of superposed flow and $\Gamma = -1$ have been presented by Gan et al. (1995), who used a different elliptic solver and a different version of the low-Reynolds-number $k-\epsilon$ turbulence model from those used in this paper. Although the two computational codes produced very similar results, for completeness some comparisons between velocity measurements and computations using the current code are shown in Figs 5 and 6.

Figure 5 shows comparisons between the computed and measured velocities for $\mathrm{Re}_\phi = 1.14 \times 10^6$ and $C_W = 4026$ ($\lambda_T = 0.0574$). The agreement is good except near $z/s = 1$, where accurate LDA measurements are difficult to make. For this value of λ_T, the measurements are outside the source region and the negative values of V_r in the core show that recirculation is occurring. The continuous shear in V_ϕ from $+\Omega r$ at $z/s = 0$ to $-\Omega r$ at $z/s = 1$ produces very little rotation in the core between the boundary layers.

Figure 6 for $\mathrm{Re}_\phi = 1.19 \times 10^6$ and $C_W = 9351$ ($\lambda_T = 0.129$) shows a distinct skew in the measured radial components of velocity, particularly at the smaller values of x. As mentioned in Section 3, gauze tubes were used in an attempt to create a uniform radial inlet; in practice, the flow impinges on the downstream disk, causing a skewed flow. Except near the disk surfaces, the measured values and computations are in better agreement at the larger values of x where inlet effects are attenuated. For $\lambda_T = 0.129$, the source region extends to $x \simeq 0.6$ (as shown in Fig. 3) and recirculation occurs at larger values of x.

Comparison between the computations and measurements at other values of Re_ϕ and C_W show similar effects to those described above. The source region increases as λ_T increases, and agreement between the computed and measured velocities tends to be better in the recirculation zone outside the source region.

4.2 Thermal Measurements. Figure 7 shows the computed and measured temperature distributions for $\Gamma = -1$ and for four values of Re_ϕ and C_W. For the heated disk ($z/s = 0$), the measured temperature and fitted curve, which provides the thermal boundary conditions for the computations, are shown. Also shown are the computed curves for the temperature of the adiabatic disk ($z/s = 1$) and for the air in the midplane ($z/s = \frac{1}{2}$). The nondimensional radius of the source region, x_e, calculated from Eq. (1.4), is also shown.

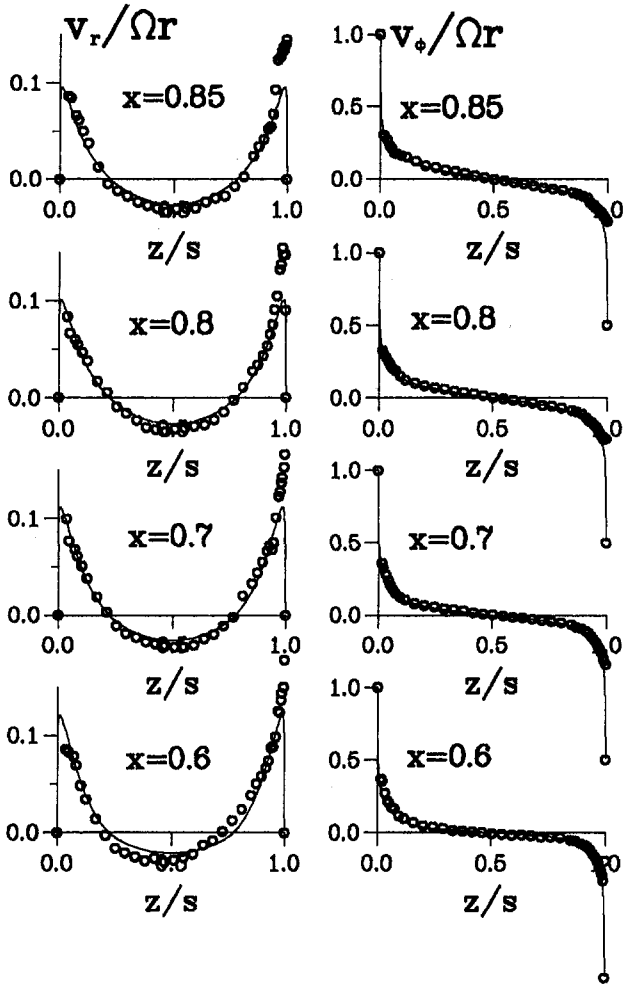

Fig. 5 Computed and measured velocity profiles for $\Gamma = -1$, $\mathrm{Re}_\phi = 1.14 \times 10^6$, and $C_W = 4026$ ($\lambda_T = 0.0574$): —— computations; ○ experimental data

Although the measured distribution of temperature on the heated disk is similar for all four cases, the computed temperatures of the adiabatic disk and the air depend strongly on λ_T. The size of the source region increases as λ_T increases, and for $x < x_e$ the temperature of the adiabatic disk is virtually equal to that of the air at inlet to the system. For $x > x_e$, the temperatures of the air and the adiabatic disk both increase with radius, the air temperature being intermediate between that of the two disks.

Figures 8–11 show comparisons between the computed and measured Nusselt numbers for $\mathrm{Re}_\phi \simeq 2 \times 10^5$ to 1.1×10^6. The uncorrected measurements are based on the fluxmeter readings, and the corrected values include the radiation correction discussed in Section 3. In Fig. 11, the Nusselt numbers for $\Gamma = 0$ (the rotor-stator results of Chen et al. 1996) are shown together with those for $\Gamma = -1$. It should be noted that the values of Re_ϕ and C_W for $\Gamma = 0$ are slightly different from the values used here for $\Gamma = -1$; it was not possible to carry out experiments at identical conditions for both cases.

Before discussing the heat transfer results, it is useful to consider the implications of the Reynolds analogy (see, for example, Owen and Rogers, 1989). For the case where the thermal boundary conditions are similar to those for the tangential component of velocity, and where the (true) *adiabatic disk temperature* is used as the reference temperature for the Nusselt number, it can be shown that the average Nusselt number is proportional to the product $C_m \mathrm{Re}_\phi$, where C_m is the moment coefficient. In Section 1, it was noted that a superposed radial

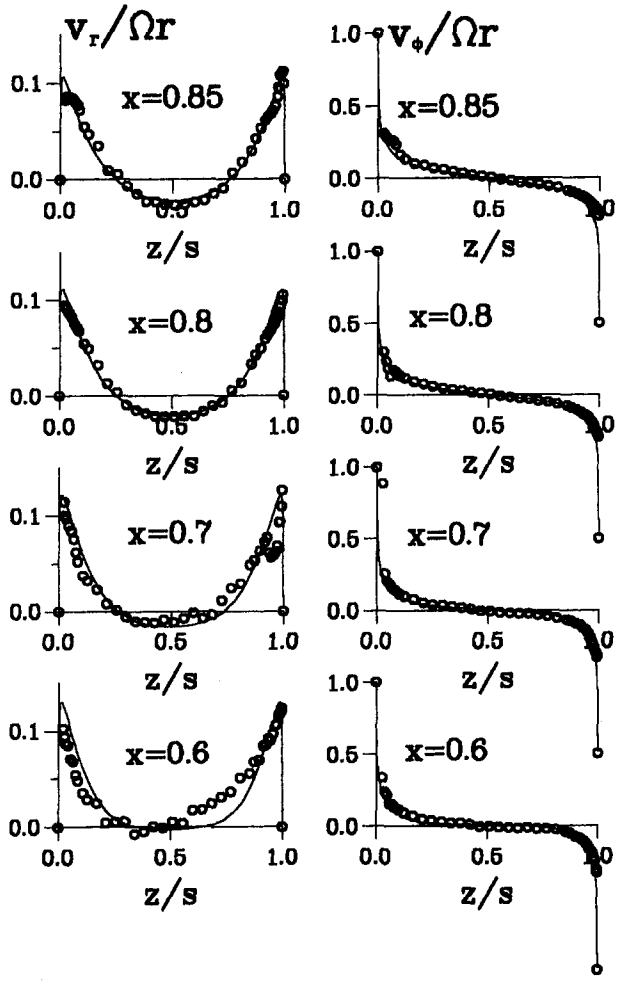

Fig. 6 Computed and measured velocity profiles for $\Gamma = -1$, $Re_\phi = 1.19 \times 10^6$, and $C_W = 9351$ ($\lambda_T = 0.129$): —— computations; ○ experimental data

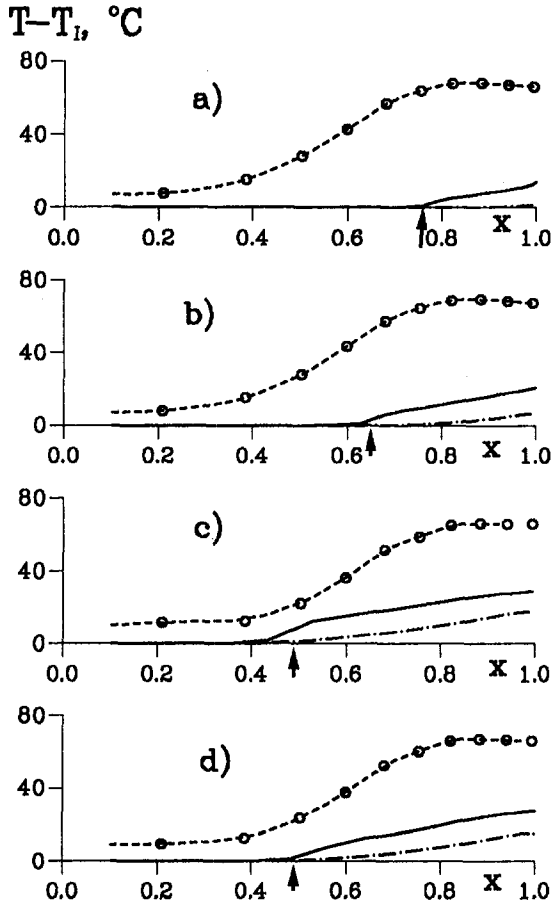

Fig. 7 Temperature distributions for $\Gamma = -1$: (*a*) $Re_\phi = 3.70 \times 10^5$, $C_W = 6128$ ($\lambda_T = 0.215$); (*b*) $Re_\phi = 3.62 \times 10^5$, $C_W = 3920$ ($\lambda_T = 0.140$); (*c*) $Re_\phi = 6.21 \times 10^5$, $C_W = 3896$ ($\lambda_T = 0.0904$); (*d*) $Re_\phi = 1.11 \times 10^6$, $C_W = 6130$ ($\lambda_T = 0.0894$); - - - heated disk (fitted); ○ measured data; — · — adiabatic disk (computed); —— air in midplane (computed) ↑ x_s (Eq. (1.4))

flow has little effect on C_m, which suggests (according to the Reynolds analogy) that the flow rate should have little effect on Nu. This is, however, an oversimplification, as the superposed flow affects the thermal boundary conditions, and the reference temperature used here is based on the inlet air temperature (which can be measured easily) and not on the local air temperature (which cannot be measured easily). It was also noted above that the size of the source region increases as λ_T increases: Inside the source region, the air temperature is close to the inlet temperature, T_I, and outside it increases with radius. Consequently, T_I is more appropriate as a reference temperature for Nu inside the source region than it is outside. It follows therefore that the Reynolds analogy is more appropriate for the larger values of λ_T, where the source region covers most of the heated disk, than for the smaller values.

Turning now to Figs. 8, 9, and 10, it can be seen that the Nusselt numbers, both measured and computed, increase with increasing Re_ϕ and with increasing radius over most of the disk surface. For a given value of Re_ϕ, the effect of C_W is relatively small, particularly for the larger values of λ_T in Figs. 8 and 9. These effects are consistent with the Reynolds analogy: In Fig. 10, the reduction in Nu with decreasing C_W is attributed to the reduction in the size of the source region and the consequent increase in the temperature of the cooling air referred to above.

The computed Nusselt numbers in Figs. 8, 9, and 10 tend to underestimate the measured values, although the agreement between the computed and corrected values of Nu improves as Re_ϕ increases: In Fig 10, the agreement is very good. For these

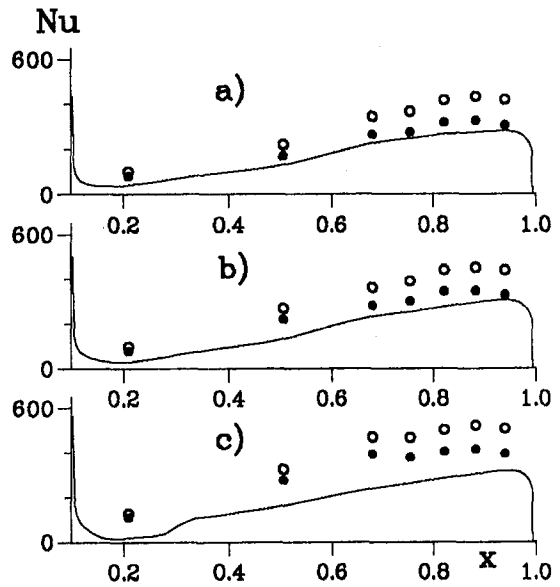

Fig. 8 Computed and measured Nusselt numbers for $\Gamma = -1$: (*a*) $Re_\phi = 2.09 \times 10^5$, $C_W = 3939$ ($\lambda_T = 0.218$); (*b*) $Re_\phi = 2.10 \times 10^5$, $C_W = 6121$ ($\lambda_T = 0.338$); (*c*) $Re_\phi = 2.24 \times 10^5$, $C_W = 9718$ ($\lambda_T = 0.510$); —— computation, ○ uncorrected data, ● corrected data

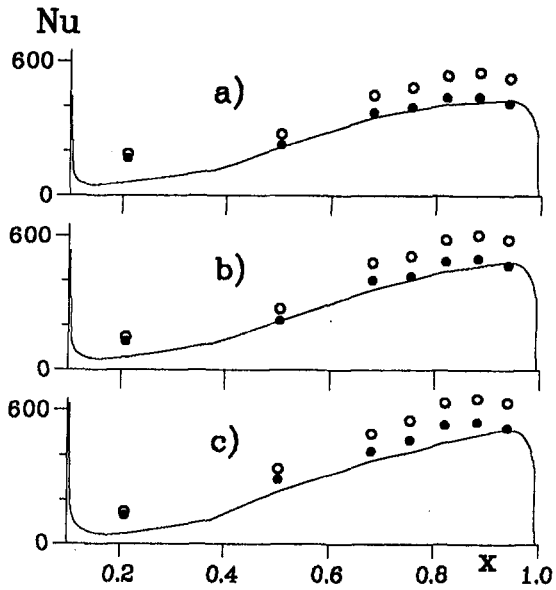

Fig. 9 Computed and measured Nusselt numbers for $\Gamma = -1$: (*a*) $Re_\phi = 3.62 \times 10^5$, $C_W = 3920$ ($\lambda_T = 0.140$); (*b*) $Re_\phi = 3.70 \times 10^5$, $C_W = 6128$ ($\lambda_T = 0.215$); (*c*) $Re_\phi = 3.84 \times 10^5$, $C_W = 9643$ ($\lambda_T = 0.329$); —— computation; ○ uncorrected data; ● corrected data

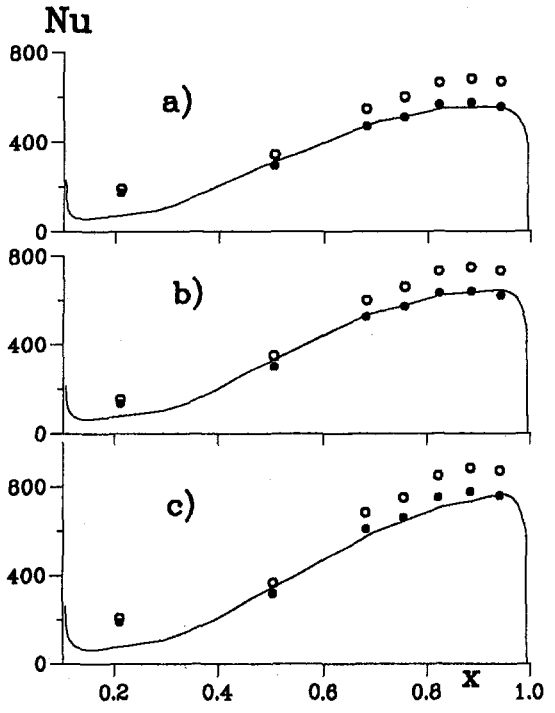

Fig. 10 Computed and measured Nusselt numbers for $\Gamma = -1$: (*a*) $Re_\phi = 6.21 \times 10^5$, $C_W = 3896$ ($\lambda_T = 0.0904$); (*b*) $Re_\phi = 6.36 \times 10^5$, $C_W = 6131$ ($\lambda_T = 0.139$); (*c*) $Re_\phi = 6.79 \times 10^5$, $C_W = 9724$ ($\lambda_T = 0.210$); —— computation; ○ uncorrected data; ● corrected data

results the computations show that the temperature of the adiabatic disk is never more than 20°C greater than T_I. As the radiation correction described in Section 3 was based on the assumption that the temperature of the unheated disk was equal to T_I, the corrected Nusselt numbers are believed to be more accurate than the uncorrected values.

Figure 11 for $Re_\phi \simeq 1.1 \times 10^6$ shows the comparison between the results for $\Gamma = -1$ and $\Gamma = 0$. Although the trends for the computational and experimental results are similar for both values of Γ, the computed and measured Nusselt numbers for

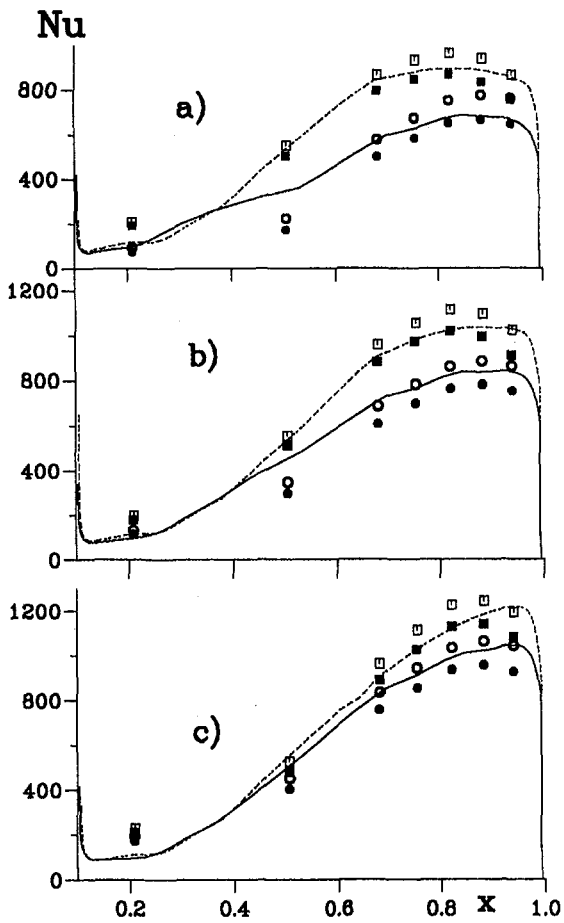

Fig. 11 Computed and measured Nusselt numbers for $\Gamma = -1$ and $\Gamma = 0$: (*a*) $Re_\phi = 1.09 \times 10^6$, $C_W = 3926$ ($\lambda_T = 0.0581$); (*b*) $Re_\phi = 1.11 \times 10^6$, $C_W = 6130$ ($\lambda_T = 0.0894$); (*c*) $Re_\phi = 1.18 \times 10^6$, $C_W = 9720$ ($\lambda_T = 0.135$); $\Gamma = -1$: —— computation, ○ data; $\Gamma = 0$: - - - computation, □ data (solid symbols refer to corrected data)

$\Gamma = 0$ are significantly higher than those for $\Gamma = -1$. It was stated in Section 1 that the value of C_m for contrarotating disks is greater than that for the equivalent rotor–stator case, although the difference reduces as the flow rate approaches the free-disk-entrainment rate. The Reynolds analogy suggests therefore that the Nusselt numbers for $\Gamma = -1$ should be *higher,* not *lower,* than those for $\Gamma = 0$. The main reason for this paradox is that, according to the computations, the air temperature in the recirculating core for $\Gamma = -1$ is higher than that in the nonrecirculating core for $\Gamma = 0$; the increase in air temperature causes a decrease in heat transfer.

In summary, the measured effects of Γ, Re_ϕ, and C_W on Nu are mainly well predicted by the computational method. The agreement is worst at the lowest Reynolds number tested ($Re_\phi \simeq 2 \times 10^5$) where the computations underpredict the measured values. For the higher values of Re_ϕ, the differences between the computations and the corrected Nusselt numbers are attributed to the uncertainties in both the computations and the measurements.

5 Conclusions

Velocity and heat transfer measurements, made in a heated rotating-disk rig with a radial outflow of cooling air, have been compared with computations made using an elliptic solver incorporating a low-Reynolds-number $k-\epsilon$ turbulence model. For $\Gamma = -1$ (the contrarotating case), comparisons are made for $Re_\phi \simeq 2 \times 10^5$ and 1.1×10^6 and $3900 < C_W < 9700$ ($0.06 < \lambda_T < 0.5$).

Both computations and experiments show trends consistent with the Reynolds analogy: For a given radial location, Nu increases strongly with Re_ϕ and weakly with C_W. The size of the source region and the temperature distribution in the cooling air depend strongly on λ_T: a large value of λ_T is associated with a large source region and with a small increase in the air temperature in the recirculation zone outside the source region.

Comparison with results for $\Gamma = 0$ (the rotor–stator case) shows that, under equivalent conditions, the Nusselt numbers for $\Gamma = -1$ are significantly less than those for $\Gamma = 0$.

Overall, the measured velocity distribution and Nusselt numbers are well predicted by the computational method.

Acknowledgments

This work has been carried out with the support of the UK Engineering and Physical Sciences Research Council and the Defence Research Agency.

References

Batchelor, G. K., 1951, "Note on a Class of Solutions of the Navier–Stokes Equations Representing Steady Rotationally-Symmetric Flow," *Quart. J. Mech. Appl. Math.,* Vol. 4, pp. 29–41.

Chen, J.-X., Owen, J. M., and Wilson, M., 1993a, "Parallel-Computing Techniques Applied to Rotor–Stator Systems: Fluid Dynamics Computations," *Proc. 8th Intl. Conf. Numer. Meth. Laminar Turbulent Flow,* Swansea, Pineridge Press, pp. 899–911.

Chen, J.-X., Owen, J. M., and Wilson, M., 1993b, "Parallel-Computing Techniques Applied to Rotor–Stator Systems: Thermal Computations," *Proc. 8th Intl. Conf. Numer. Meth. Thermal Problems,* Swansea, Pineridge Press, pp. 1212–1226.

Chen, J.-X., Gan, X., and Owen, J. M., 1996, "Heat Transfer in an Air-Cooled Rotor–Stator System," ASME JOURNAL OF TURBOMACHINERY, Vol. 118, pp. 444–451.

Dorfman, L. A., 1963, *Hydrodynamic Resistance and the Heat Loss of Rotating Solids,* Oliver and Boyd, Edinburgh.

Gan, X., Kilic, M., and Owen, J. M., 1995, "Flow Between Contrarotating Discs," ASME JOURNAL OF TURBOMACHINERY, Vol. 117, pp. 298–305.

Graber, D. J., Daniels, W. A., and Johnson, B. V., 1987, "Disk Pumping Test," Air Force Wright Aeronaut. Lab., Report No. AFWAL-TR-87-2050.

Kilic, M., Gan, X., and Owen, J. M., 1994a, "Superposed Flow Between Two Discs Contrarotating at Differential Speeds," *Int. J. Heat Fluid Flow,* Vol. 15, pp. 438–446.

Kilic, M., Gan, X., and Owen, J. M., 1994b, "Transitional Flow Between Contrarotating Discs," *J. Fluid Mech.,* Vol. 281, pp. 119–135.

Kilic, M., Gan, X., and Owen, J. M., 1996, "Turbulent Flow Between Two Discs Contrarotating at Different Speeds," ASME JOURNAL OF TURBOMACHINERY, Vol. 118, pp. 408–413.

Morse, A. P., 1988, "Numerical Prediction of Turbulent Flow in Rotating Cavities," ASME JOURNAL OF TURBOMACHINERY, Vol. 110, pp. 202–215.

Morse, A. P., 1991, "Application of a Low Reynolds Number $k-\epsilon$ Turbulence Model to High-Speed Rotating Cavity Flows," ASME JOURNAL OF TURBOMACHINERY, Vol. 113, pp. 98–105.

Owen, J. M., and Rogers, R. H., 1989, *Flow and Heat Transfer in Rotating Disc Systems, Vol. 1: Rotor Stator Systems,* Research Studies Press, Taunton (Wiley, New York).

Stewartson, K., 1953, "On the Flow Between Two Rotating Coaxial Disks," *Proc. Camb. Phil. Soc.,* Vol. 49, pp. 333–341.